A continuum one-dimensional SOC model for thermal transport in tokamaks

2003 Nucl. Fusion 43 1740

(http://iopscience.iop.org/0029-5515/43/12/018)

INSTITUTE OF PHYSICS PUBLISHING and INTERNATIONAL ATOMIC ENERGY AGENCY NUCLEAR FUSION

Nucl. Fusion **43** (2003) 1740–1747 PII: S0029-5515(03)69595-5

A continuum one-dimensional SOC model for thermal transport in tokamaks

Varun Tangri, Amita Das, Predhiman Kaw and Raghvendra Singh

Institute for Plasma Research, Bhat, Gandhinagar, 382428, India

Received 18 November 2002, accepted for publication 27 August 2003
Published 1 December 2003
Online at stacks.iop.org/NF/43/1740

Abstract

Based on the now well-known and experimentally observed critical gradient length (L_{Te}) in tokamaks, we present a continuum one-dimensional model for explaining self organized heat transport in tokamaks. The key parameters of this model include a hysteresis parameter, which ensures that the switching of the heat transport coefficient χ upwards and downwards takes place at two different values of R/L_{Te}. Extensive numerical simulations of this model reproduce many features of present day tokamaks, such as sub-marginal temperature profiles, intermittent transport events, $1/f$ scaling of the frequency spectra, propagating fronts, etc. This model utilizes a minimal set of phenomenological parameters, which may be determined from experiments and/or simulations. Analytical and physical understanding of the observed features has also been attempted.

PACS numbers: 52.25.Fi, 52.25.Gj, 52.55.Fa

1. Introduction

Recent experimental work on turbulence driven heat transport in tokamaks has revealed many features that are consistent with a self-organized criticality (SOC) [1,2] model of transport [3]. Notable among these features (e.g. for electron heat transport) are: (i) observation of a threshold [4] (typically sub-marginal) temperature profile with a strong tendency towards 'profile consistency' [5, 6] (i.e. relative insensitivity of the measured profile shape to the radial distribution of heat source); (ii) large scale intermittent transport events (as revealed by electron cyclotron emission measurements) exhibiting long time auto-correlations [7]; (iii) characteristic frequency spectra showing scaling behaviour, $f^{-\alpha}$ with $\alpha \sim 1$ [8]; (iv) observation of non-diffusive radial propagation of fronts associated with avalanche events with speeds of the order of a few hundred metres per second [9] etc. Most of the features discussed above are generic for turbulent transport in toroidal devices and have also been observed in studies of core ion transport, edge heat transport, flux driven scrape-off layer transport [7–18], etc. Full scale, three-dimensional gyrofluid and gyro-kinetic simulations of tokamak plasmas describe the basic temperature gradient driven instability (e.g. electron temperature gradient, ETG) and related modulational instabilities leading to generation of zonal flows, streamers, etc [19]. Although such simulations [20] reproduce many observed features of heat transport, they are so complex that important physics gets obscured. Cellular automata models [21] that are oversimplified and discrete also fail to highlight relevant physical issues. What is needed is a simplified physical model that can bridge the gap and elucidate important points.

Such diverse observations made earlier, can be unified through a simple generic one-dimensional continuum model, which forms the basis of this paper. We have observed that this simple model set of equations is able to reproduce all the features of the transport discussed earlier in terms of a few phenomenological parameters. With appropriate modifications, this model can also be applied to many other observations in magnetized plasmas like ion thermal transport, edge localized modes (ELMS), flux driven transport in scrape-off layers, etc.

We offer an analytical description of some of the observed phenomena and also discuss how the key phenomenological parameters may be obtained from experiments and/or detailed three-dimensional computer simulations.

The remaining part of this article is organized as follows: section 2 describes the basic model used and the results are presented in section 3. The final conclusions are discussed in section 4.

2. Basic formulation

Using a set of two coupled equations [23], we retain an essential aspect of the ETG transport model: a critical gradient length below which transport assumes a high value. The first of these is a one-dimensional radial transport equation with sources and the second a nonlinear relaxation equation for the turbulence

driven transport coefficient χ:

$$\frac{\partial T}{\partial t} = \frac{\partial}{\partial x}\left(\chi \frac{\partial T}{\partial x}\right) + S(x,t) \tag{1}$$

$$\frac{\partial \chi}{\partial t} + \chi = Q\left(x, t, \frac{\partial T}{\partial x}\right) \tag{2}$$

where we have used normalized variables $T = \bar{T}/T_0$, $x = \bar{x}/x_0$, $t = \bar{t}/\tau$, $\chi = \bar{\chi}\tau/x_0^2$, $S = P\tau/(3nT_0/2)$. P is the input power density that determines the source S, n is the plasma density, x_0 and T_0 are normalizing variables and τ is the natural nonlinear relaxation time of the χ equation.

The source function Q for χ is designed to mimic the behaviour of ETG by switching it between two values $\chi_{\max}$ and $\chi_{\min}$. SOC features are incorporated into the picture through a hysteresis parameter β. The following special forms of the function Q form the focus of this paper:

$$Q = \begin{cases} \chi_{\max} & \text{if } \dfrac{\mathrm{d}T}{\mathrm{d}x} > k \\ \chi_{\min} & \text{if } \dfrac{\mathrm{d}T}{\mathrm{d}x} < \beta k \end{cases} \tag{3a}$$

$$Q = \begin{cases} \chi_{\max} & \text{if } \dfrac{1}{T}\dfrac{\mathrm{d}T}{\mathrm{d}x} > k \\ \chi_{\min} & \text{if } \dfrac{1}{T}\dfrac{\mathrm{d}T}{\mathrm{d}x} < \beta k \end{cases} \tag{3b}$$

Hysteresis ensures that the switch of χ upwards and downwards takes place at two different thresholds: k and βk. Thus, Q changes from $\chi_{\min}$ to $\chi_{\max}$ when ∇T (or $(1/T)\nabla T$) exceeds a critical value k but switches back from $\chi_{\max}$ to $\chi_{\min}$ only if ∇T (or $(1/T)\nabla T$) is less than βk; β is the hysteresis parameter and takes values less than 1. The presence of hysteresis (i.e. $\beta \neq 1$) in the source function Q is crucial for the depiction of SOC characteristics; hysteresis is related to the physical fact that once the turbulence is excited it may be possible to sustain it even when ∇T goes below the linear instability threshold.

We have not yet justified the use of two forms for the function Q. The first of these is from an adaptation of an earlier work by Lu [24] on solar flares to heat transport in tokamaks.

The second model is based on analytical calculations of electron heat transport [26–28] which have shown that when $\eta_e = \mathrm{d}\ln T/\mathrm{d}\ln n$ exceeds a critical value, short scale, fast growing electrostatic modes generally known as the ETG modes are excited. These modes leave the ion transport unaffected and enhance the electron thermal conductivity χ. Experiments, linear and nonlinear theories of this mode generally give χ_{ETG} of the following form [28, 29, 22, 4]:

$$\chi_{\mathrm{ETG}} = \chi_{\min} + \chi_{\max} G\left(\frac{R}{L_{\mathrm{Te}}} - \left(\frac{R}{L_{\mathrm{Te}}}\right)_{\mathrm{c}}\right) \tag{3}$$

where G is the Heaviside step function $G(x) = 1\ \forall x > 0$ and $G(x) = 0\ \forall x \leqslant 0$, $L_{\mathrm{Te}} = T/\nabla T$ is the gradient length and R the major radius. $\chi_{\min}$ is the transport coefficient in the absence of temperature gradient turbulence and $\chi_{\max}$ is the transport coefficient associated with saturated ETG turbulence which may include effects due to generation of zonal flow streamers, etc.

In the next section, we present results of our simulations for $\beta \neq 1$. Section 3.1 discusses results using equation 3(a) and section 3.2 discusses those using 3(b).

3. Numerical experiments

We now make rough estimates of values for the parameters $\chi_{\min}$, $\chi_{\max}$ and τ for use in numerical experiments. We have chosen the ratio of $\chi_{\max}/\chi_{\min}$ from experimental data. For example, Ryter *et al* [22] have presented data on χ_e versus R/L_{Te} (see figure 4 of [22]). Not only does it suggest a critical value L_{Te}, it also suggests that $\bar{\chi}_{\max}/\bar{\chi}_{\min} \sim 10$.

The parameter $\bar{\chi}_{\max}(=\chi_{\max}x_0^2/\tau)$ is the anomalous transport associated with the ETG turbulence once the gradient exceeds a critical value. Because of frequent avalanches, χ never attains this upper limit. Thus, $\bar{\chi}_{\max} \sim 3\bar{\chi}_{\mathrm{meas}}$ and is taken as $10^5\ \mathrm{cm^2\ s^{-1}}$. Hence, the minimum value $\bar{\chi}_{\min} = \bar{\chi}_{\max}/10 \sim 10^4\ \mathrm{cm^2\ s^{-1}}$.

τ being a relaxation time for the ETG turbulence, describes the time taken by χ to stabilize at $\chi_{\max}$ after ∇T crosses the critical value k. This involves saturation of the ETG turbulence, growth of streamer like modulational instabilities (since they are suspected to dominate the ETG transport [19]) and their saturation by Kelvin–Helmholtz secondary instabilities. An estimate of τ can be obtained from large scale simulations and/or from experiments [19]; they give a value of the order of $\tau \sim 10^3 L_T/V_{\mathrm{th}} \approx 100\,\mu\mathrm{s}$ where V_{th}/L_T is the typical ETG growth rate.

We have numerically solved equations (1) and (2) by finite differencing in space and the time advancement is carried out by the gear method with 401 grid points. We present results for the case when the source function is of the form $S(x) = S_0 \sin(\pi x/2L)$. In addition to the above case, we have also carried out simulations with other forms of $S(x)$. These include: (i) random, (ii) strongly localized, peaked Gaussian profiles. In each of these cases, sub-marginal temperature profiles with non-Gaussian intermittent transport events emanating the added energy were seen. Roughly speaking, we can say that the form of $S(x)$ is not important. The box size has been fixed at $L = 20$, the values of the critical slope parameter $k = 0.04$ (section 3.1) and $k = 0.25$ (section 3.2), and the hysteresis parameter $\beta = 0.9$. $\chi_{\max}$ and $\chi_{\min}$ are chosen to be 2 and 0.2, respectively, and S_0 is chosen in the range 10^{-3}–10^{-2}. As explained later, these dimensionless values correspond to typical numbers characteristic of tokamaks like JET, TORE-SUPRA and D-III D.

3.1. Critical gradient based model

The numerical solution of equations (1), (2) and 3(a) show consistency with many observations. The plot in figure 1 shows clearly that the profile of T (after an initial transient state) approaches a state where ∇T is below the critical slope at nearly all points. In our numerical experiments we performed a number of simulations with various initial profiles that were either (1) nearly linear, $T(x) \sim kx + \tilde{T}$, where $\tilde{T}$ is a perturbation, or (2) random, with $T(x)$, satisfying the boundary conditions. In each of these cases, the instantaneous T profile

very rapidly approaches a sub-critical state. This result is consistent with the experimental observation of sub-marginal temperature profiles. As indicated in the previous section, we have also used different forms of the source function $S(x)$ (shown in figure 1(a)) and found little effect on the temperature profile (indicated in figure 1(b)). This is similar to observation of profile resilience in tokamaks. Furthermore, in time, a complex sequence of avalanches carrying the flux of T through the system are observed, as required for the SOC state. The detailed results obtained using this model can be summarized as follows: (i) The simulations show (figure 2(a)) propagating front like structures in the gradient of T field (as well as in the diffusivity χ) propagating in both directions. These fronts propagate with a constant velocity $\bar{U}$. (ii) The velocity $\bar{U}$ is found to scale as $\sqrt{\chi_{\max}/\tau}$ (figures 2(b) and (c)). (iii) The total energy of the system, defined by $E(t) = \int \mathrm{d}x\, T^2(x,t)$ (which is like the thermal energy nT if $n(x)$ and $T(x)$ are taken to be identical functions for simplicity), shows quasi-periodic behaviour with a steady linear rise with time (loading) and a sudden crash (unloading) displaying a saw tooth form (figure 3(a)). (iv) The amplitude $\Delta E = E_{\max} - E_{\min}$ and the frequency ν of such saw tooth events are, in general, of statistical nature. However, their mean values are observed to depend on the parameters $\chi_{\min}$ and the source strength S_{o}. When S_{o} becomes large ($S_{\mathrm{o}} \sim 5 \times 10^{-3}$ in our simulations), the frequency of saw tooth events becomes comparable to the crash time. Beyond this S_{o}, the saw toothing disappears and a general effervescence (a random time dependence) of $E(t)$ is observed. (v) The value of ΔE and ν also depend on the hysteresis parameter β. The mean value $\langle \Delta E \rangle$ scales linearly with $(1 - \beta^2)$ (figure 3(b)). We note that the model makes predictions that are in conformity with special features of electron thermal transport in tokamaks. Thus, observations (i) and (ii) are related to the radial propagation of avalanche fronts across a discharge, and observations (iii)–(v) show the intermittent, 'bursty' nature of the transport (figure 3(c)).

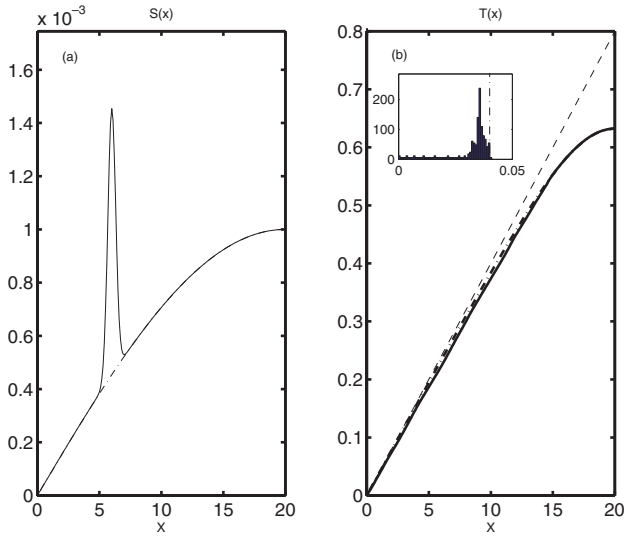

Figure 1. Different source functions as shown by solid and dash-dotted lines with corresponding relaxed T profiles in (b). The inset shows the PDF from the spatial distribution of the temperature gradient $\partial T/\partial x$. The straight (- - - -) lines indicate the critical profile.

Lu's model of SOC [24] has in part been adapted to the reconnection problem in magnetic substorms by Klimas *et al* [25]. While the observations (i), (iii) and (iv) above are similar to those obtained earlier by Klimas *et al* [25], for the sub-storm problem, (ii) and (v) are new results and have been obtained by us after extensive numerical simulations. Klimas *et al* [25] and Lu [24] also do not attempt to provide any detailed explanation of many of their observations. Our paper thus adds to the detailed study of this model by providing qualitatively new results as well as giving a quantitative interpretation of old as well as new results.

The observed scaling of the propagation speed of fronts can be understood from the following simplified analysis. The

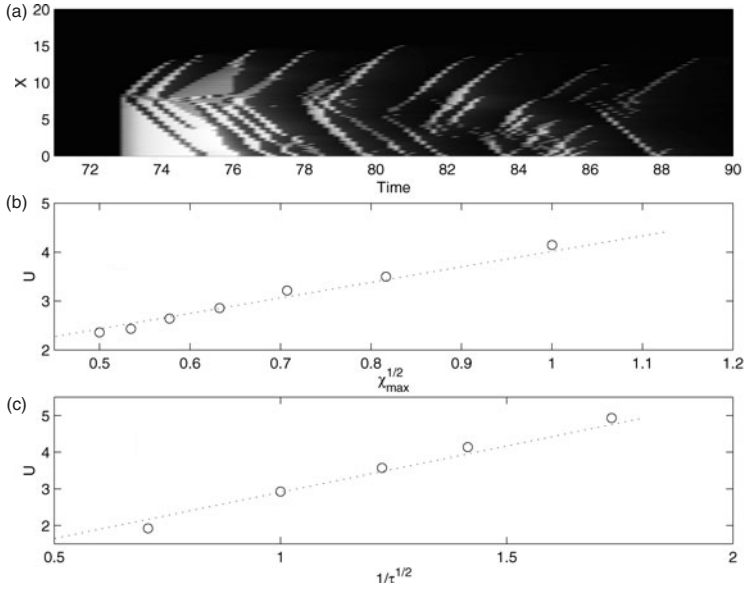

Figure 2. (a)Propagating fronts of diffusivity χ with light areas indicating high χ. The variation of velocity of fronts U with (b) varying $\chi_{\max}$, (c) varying $1/\tau^{1/2}$.

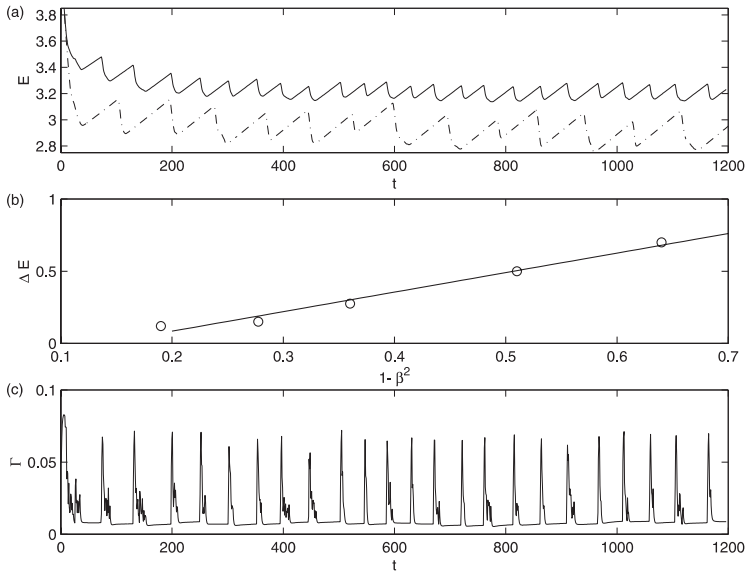

Figure 3. Loading–unloading cycle: (*a*) plot of E versus time; (*b*) mean cycle amplitude ΔE versus $1-\beta^2$; (*c*) evolution of flux at $x = 0.1$.

front structure in the diffusion coefficient arises due to the switching of Q from $\chi_{\min}$ to $\chi_{\max}$, at locations where the local slope exceeds the critical value k. The subsequent evolution of the diffusivity with time (so long as Q remains at $\chi_{\max}$), as governed by equation (2), is given by the following expression:

$$\chi(t) = \chi_{\max}\{1 - \exp(-t)\} + \chi_{\min}\exp(-t) \qquad (4)$$

For $\chi_{\min} \ll \chi_{\max}$ (as indeed is the case) and for a time $t \ll 1$ we can approximate the expression for χ as $\chi = \chi_{\max} t$. We may now write the diffusion equation as $\partial T/\partial\eta = \partial^2 T/\partial x^2$, where $\eta = \chi_{\max} t^2/2$; the exact solution shows diffusion in $x - \eta$ variables, $x^2 \approx \eta \approx \chi_{\max} t^2/2$ giving a front propagation speed in dimensional variables, $\bar{U} = \bar{x}/\bar{t} \approx \sqrt{\bar{\chi}_{\max}/2\tau}$. Figures 2(*b*) and (*c*) give plots illustrating this scaling as observed in the numerical simulations.

The quasi-periodic oscillations of energy (figure 3(*a*)) having a saw tooth character in time, signify a slow building up of the temperature profile from βkx towards kx by the source function followed by a sudden crash. The maximum amount of energy that can be released by the system in a crash can be estimated from the difference of the energies of the two states. The state $T = \beta kx$, thus defines the minimum energy and is given by $E_{\min} = \int T^2\,\mathrm{d}x = \beta^2 k^2 \int x^2\,\mathrm{d}x = \beta^2 k^2 L^3/3$. On the other hand, the maximum energy that can be retained by the system so that $T = kx$ is given by $E_{\max} = \int T^2 \mathrm{d}x = k^2 \int x^2 \mathrm{d}x = k^2 L^3/3$. The difference $\Delta E = E_{\max} - E_{\min} = (1-\beta^2)E_{\max} = (1-\beta^2)k^2(L^3/3)$ gives the maximum amplitude of ΔE in the growth and decay cycle that the system can exhibit. The observed amplitudes, in general, are typically lower than the above estimate because L, the box size, should be replaced by l representing the typical avalanche size in the above expression. Thus, the average energy release in the avalanches is $\langle\Delta E\rangle = (1-\beta^2)k^2\bar{l}^3/3$, (assuming $\bar{l}$ is independent of β) confirming the observed scaling with β that can be seen from the plot of figure 3(*b*) and mentioned earlier in point (v) of the summary of results.

The parameter $\chi_{\min}$ essentially determines the spatial correlation length l_c for T (note that for $\chi_{\min} = 0$ during the growth phase, equation (1) turns into an ordinary differential, i.e. $l_c = 0$). As $\chi_{\min}$ is increased it correlates T over disparate spatial regions by diffusion. Thus, a high value of $\chi_{\min}$ might seem desirable.

We now discuss in somewhat more detail the implications of the results of this model for the electron thermal transport in tokamaks. First, we look at some numbers. If we take $x_0 = 2.5\,\mathrm{cm}$, $T_0 = 10\,\mathrm{keV}$, $\tau \approx 10^{-4}\,\mathrm{s}$, $\bar{\chi}_{\max} \approx 10^5\,\mathrm{cm^2\,s^{-1}}$, $n \approx 10^{13} \times 5\,\mathrm{cm^{-3}}$ and $P \approx 1\,\mathrm{MW\,m^{-3}}$, we are considering a 50 cm radius plasma with a peak temperature of about 8 keV with ≈10 MW of input power which is like the plasma in the Tore Supra experiment; this choice gives us dimensionless parameters $L = 20$, $S = 10^{-3}$, $\chi_{\max} \approx 2$ as shown in our sample simulation. Experiments like JET and D-III D also give a similar parameter range for the simulations. Inserting these values into the formula $\bar{U} = \sqrt{\bar{\chi}_{\max}/2\tau}$, we obtain a speed of the order of $200\,\mathrm{m\,s^{-1}}$ for the radial propagation of avalanche like fronts, as in the experiment by Politzer *et al* [9]. It must be noted that other models [13–15] also predict ballistic propagation of matter or energy in tokamak plasmas.

3.2. Critical gradient length based model

This section presents results from simulations of a one-dimensional transport model using a critical gradient length L_{Te} below which the transport has a high value. As before, we consider a 50 cm radius plasma with a peak temperature of about 8 keV. We have followed the earlier choice of parameters except for $k = 0.25$, $T_o = 0.1\,\mathrm{keV}$ and $P = 1.2\,\mathrm{MW}$ along with the boundary conditions $(\partial T/\partial x)(x = L) = 0$ and $\chi(\partial T/\partial x)(x = 0) = \int S(x)\,\mathrm{d}x$. Note that the $x = 0$ boundary (edge) is assumed to emit flux. Again the initial profile was chosen to be close to the critical profile to ensure a quick relaxation with as few transients as possible. The choice of other initial profiles indicates similar results, but these take a little longer time to relax to a sub-marginal profile.

Figure 4(*a*) shows a typical instantaneous profile from our simulations. As shown in figure 4(*b*), the probability distribution function (PDF) of $\nabla T/T$ indicates

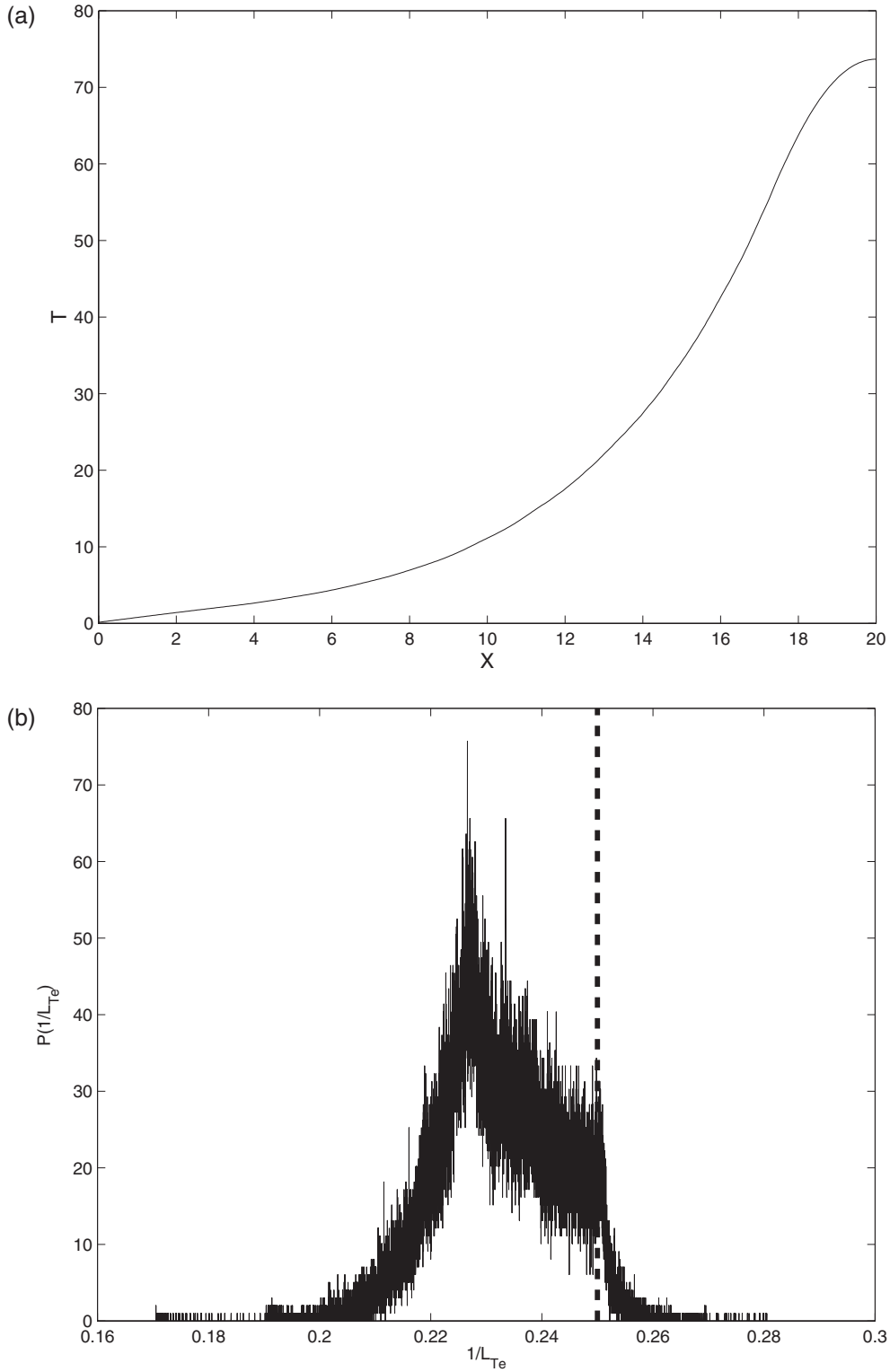

Figure 4. (*a*) Typical instantaneous profile from simulation; (*b*) the probability distribution of the $1/L_{\mathrm{Te}} = \nabla T/T$ from a time series accumulated at a point ($x = 9.95$).

sub-marginality—the most probable value of $\nabla T/T$ lies below k. The dashed line indicates the critical value k. The observation that $1/L_{\mathrm{Te}}$ mostly lies below this line reinforces the earlier fact. The flux shows greater intermittency than the previous model (section 3.1). Hence, in this section, we mainly concentrate on the characteristics of turbulent flux $\Gamma(x,t) = \chi(x,t)\partial T/\partial x$. The typical evolution of this quantity is similar to that shown in figure 5(*a*).

The power spectra obtained from the time series of flux (figure 5(*b*)) indicates a $1/f^{\alpha}$ (with $\alpha \sim 1$) type of power spectrum. Experimental observations on various tokamaks (see, e.g. Politzer *et al* [9], Pedrosa *et al* [10]), numerical

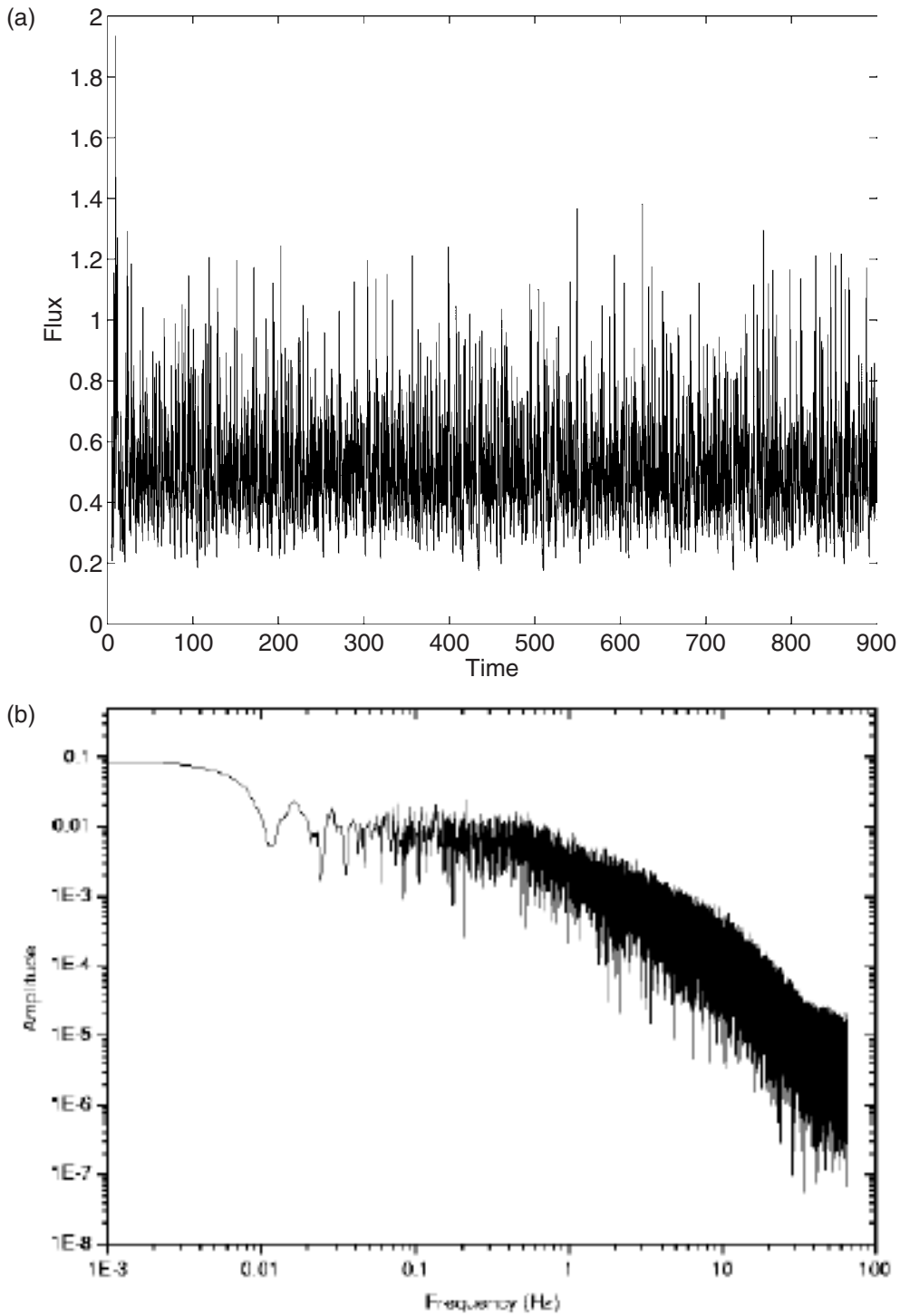

Figure 5. Time evolution of flux and its spectrum at $x = 14.95$.

simulations [21, 20, 11] and cellular automata models have reported similar spectra.

Along with a power law tail, the Hurst parameter H, also characterizes such events (Politzer *et al* [9] and references therein) and has assumed significant importance in tokamak experiments [7]. Using the data presented here, we calculated the Hurst parameter and found it to be different at different locations. We have calculated the Hurst parameter from our simulation data by the method of R/S statistics at $x = 10$. After R/S data points with the least statistical value (i.e. the smallest n and the largest n) have been neglected, we arrive at a value $H = 0.87$. Having H so close to 1 indicates that events are occurring on all timescales, down to the size of the numerical time step. The value obtained by us is somewhat larger than that obtained from actual experiments (Politzer *et al* [8]). The two-dimensional graph of Γ versus t having a nonzero H also possesses a fractal dimension D. In fact $D = 2 - H$ (Peitgen *et al* [30]). Thus, $D = 1.13$.

To further analyse our studies of the statistical properties of flux as obtained from our system of equations, we have also obtained the PDF of the flux. We define the PDF $P(\Gamma_T) = N_{\Gamma_T}/NW$, where N_{Γ_T} is the number of data values that fall between Γ_T and $\Gamma_T + W$, W is a narrow interval starting at Γ_T and N is the total number of data values. Figure 6 shows the PDF of a flux time series accumulated at a point ($x = 14.95$). The PDF displays striking non-Gaussian features. To further examine such features, we have superimposed a Gaussian distribution function of the same peak value, mean and standard deviation. The distance between the two points (denoted by $*$) is about 2σ, where σ is the standard deviation. The PDF has an exponential tail as indicated by the straight line fit. Quantitatively, events of magnitude more than 4σ are nearly twenty times more probable than a Gaussian.

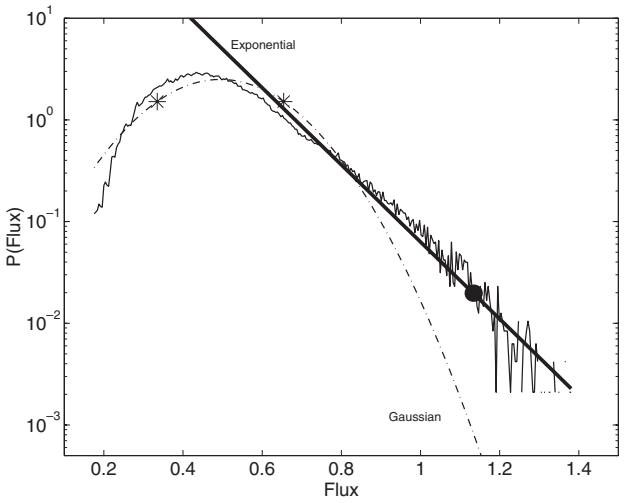

Figure 6. PDF $P(\Gamma_T)$. The dash-dotted line represents a Gaussian with the same mean and standard deviation. The solid line is an exponential fit for the tail.

To further characterize the PDF, we have obtained the profiles of skewness and kurtosis as well (figure 7). As in previous experiments and simulations [31, 32], we find a positive skewness and a kurtosis more than 3. Note that for a Gaussian distribution, the skewness must be 0 and kurtosis 3.

4. Conclusions

We have reproduced many observed features of electron heat transport by the numerical solution of a one-dimensional model. The model involves radial transport driven by ETG at a critical gradient length. Hysteresis introduces many features that are consistent with the picture of SOC. These include: (i) sub-marginal temperature profiles, (ii) profile resilience, (iii) intermittent large scale transport events, (iv) power spectrum, (v) radially propagating fronts with speeds of order $(\bar{\chi}_{\max}/2\tau)^{1/2} \sim 200\,\mathrm{m\,s^{-1}}$ and (vi) measurements of the PDF of flux and the Hurst parameter indicate occurrence of avalanche events on all timescales.

It would be interesting to verify the physics described here and to determine the phenomenological parameters introduced. There is already abundant experimental data on the critical threshold gradient length L_{Te}. Active experiments with localized heat sources like ECRH could be carried out to measure $\chi_{\max}$, $\chi_{\min}$, the relaxation time τ, the hysteresis parameter β, etc. Similarly, simulations and analytical theory could be used to understand the magnitudes of these phenomenological parameters and would thus elucidate the physics of the phenomenon a little better.

Finally, we emphasize that the paradigm introduced here for electron thermal transport is much more general and may be applicable to a number of observations in magnetically confined plasmas (with appropriate modifications) such as ELMS, flux driven transport in scrape-off layers, ion thermal transport and particle transport in core regions, etc. It may also be useful to extend these one-dimensional models to situations

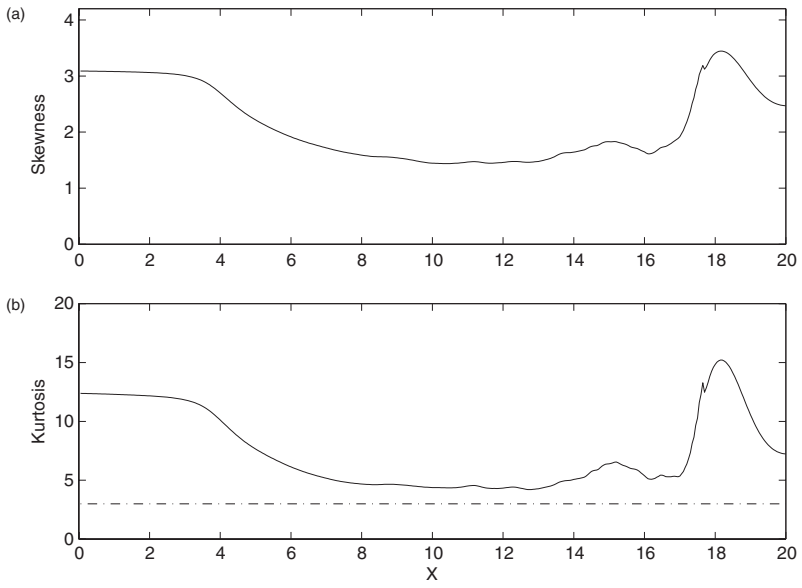

Figure 7. Profiles of skewness and kurtosis. The dash-dotted line has kurtosis =3.

involving coupled transport equations in density, temperatures, currents, etc.

Acknowledgments

A.D. and P.K. are grateful to Xavier Garbet and other organizers of the Workshop on Self Organization and Transport in Electromagnetic Turbulence, July 2001 at Aix-en-Provence, France where this work was initiated.

References

[1] Bak P., Tang C. and Wiesenfeld K. 1987 *Phys. Rev. Lett.* **59** 381
[2] Bak P., Tang C. and Wiesenfeld K. 1988 *Phys. Rev.* A **38** 364
[3] Diamond P.H. and Hahm T.S. 1995 *Phys. Plasmas* **2** 3640
[4] Hoang G.T. *et al* 2001 *Phys. Rev. Lett.* **87** 125001
[5] Ryter F. *et al* 2001 *Phys. Rev. Lett.* **86** 2325
[6] Ohyabu N. *et al* 2002 *Plasma Phys. Control. Fusion* **44** A211–16
[7] Carreras B.A. *et al* 1998 *Phys. Rev. Lett.* **80** 4438
[8] Politzer P.A. *et al* 2002 *Phys. Plasmas* **9** 1962
[9] Politzer P.A. 2000 *Phys. Rev. Lett.* **84** 1192
[10] Pedrosa M.A. *et al* 1999 *Phys. Rev. Lett.* **82** 3621
[11] Sarazin Y. and Ghendrih Ph. 1998 *Phys. Plasmas* **5** 4214
[12] Garbet X. and Waltz R.E. 1998 *Phys. Plasmas* **5** 2836
[13] Diamond P.H. *et al* 1995 *Phys. Plasmas* **2** 3640
[14] Diamond P.H. *et al* 1995 *Phys. Plasmas* **2** 3685
[15] Sarazin Y. *et al* 2000 *Phys. Plasmas* **7** 1085
[16] Antar G.Y. *et al* 2001 *Phys. Plasmas* **8** 1612
[17] Jha R. *et al* 1992 *Phys. Rev. Lett.* **69** 1375
[18] Beyer P. *et al* 2000 *Phys. Rev. Lett.* **85** 4892
[19] Dorland W., Jenko F., Kotschenreuther M. and Rogers B.N. 2000 *Phys. Rev. Lett.* **85** 5579
[20] Carreras B.A. *et al* 1996 *Phys. Plasmas* **3** 2903
[21] Newman D.E. *et al* 1996 *Phys. Plasmas* **3** 1858
[22] Ryter F. *et al* 2001 *Plasma Phys. Control. Fusion* **43** A323
[23] Tangri V. *et al* 2003 *Phys. Rev. Lett.* **91** 025001
[24] Lu E.T. 1995 *Phys. Rev. Lett.* **74** 2511
[25] Klimas A.J. *et al* 2000 *J. Geophys. Res.* **105** 18765
[26] Singh R. *et al* 2001 *Phys. Plasmas* **8** 4340
Singh R. *et al Nucl. Fusion* **41** 1219
[27] Horton W. *et al* 1998 *Phys. Fluids* **31** 2971
[28] Dong J.Q. *et al* 2002 *Phys. Plasmas* **9** 4699
[29] Kotschenreuther M. *et al* 1995 *Phys. Plasmas* **2** 2381
[30] Peitgen *et al* 1992 *Chaos and Fractals* (Berlin: Springer) p 495
[31] Carreras B.A. *et al* 1996 *Phys. Plasmas* **3** 2664
[32] Sarazin Y. *et al* 2003 *J. Nucl. Mater.* **313–316** 796